Applied Materials Today 36 (2024) 102056

Contents lists available at ScienceDirect

Applied Materials Today

journal homepage: www.elsevier.com/locate/apmt

Plasma-enabled multifunctional platform for gram-scale production of graphene and derivatives

Ana Dias [a,*], Edgar Felizardo [a], Neli Bundaleska [a], Miroslav Abrashev [b], Jivko Kissovski [b], Ana M. Ferraria [c], Ana M. Rego [c], Thomas Strunskus [d], Patrícia A. Carvalho [e], Amélia Almeida [f], Janez Zavašnik [g], Eva Kovacevic [h], Johannes Berndt [h], Nenad Bundaleski [i], Mohammed-Ramzi Ammar [j], Orlando M.N.D. Teodoro [g], Uroš Cvelbar [g], Luís L. Alves [a], Bruno Gonçalves [a], Elena Tatarova [a,*]

[a] Instituto de Plasmas e Fusão Nuclear, Instituto Superior Técnico, Universidade de Lisboa, Av. Rovisco Pais 1, Lisbon 1049-001, Portugal
[b] Faculty of Physics, Sofia University, 1 James Bourchier Blvd., Sofia 1164, Bulgaria
[c] BSIRG, IBB - Institute for Bioengineering and Biosciences, Departamento de Engenharia Química, and Associate Laboratory i4HB—Institute for Health and Bioeconomy at Instituto Superior Técnico, Universidade de Lisboa, Av. Rovisco Pais 1, Lisbon 1049-001, Portugal
[d] Chair for Multicomponent Materials, Institute for Materials Science, Christian Albrechts Universitaet zu Kiel, Kaiserstr. 2, Kiel 24143, Germany
[e] SINTEF Industri, Materials Physics, Forskningsveien 1, Oslo 0373, Norway
[f] Centre of Physics and Engineering of Advanced Materials, Instituto Superior Técnico, Universidade de Lisboa, Av. Rovisco Pais 1, Lisbon 1049-001, Portugal
[g] Department of Gaseous Electronics F6, Jozef Stefan Institute, Jamova cesta 39, Ljubljana 1000, Slovenia
[h] GREMI UMR 7344 CNRS and Université d'Orléans, 14 rue d'Issoudun, Orléans 45067, France
[i] CEFITEC, Departamento de Física, Faculdade de Ciências e Tecnologia, Universidade Nova de Lisboa, Quinta da Torre, Caparica 2829-516, Portugal
[j] ICMN UMR7374, CNRS & Université d'Orléans, 45071, Orléans Cedex 2, France

ARTICLE INFO

Keywords:
Microwave plasmas
Self-assembly
Graphene/n-graphene
Hybrids
Graphene applications

ABSTRACT

Taking advantage of the high-energy-density microwave plasma environment as a unique 3D space for the self-assembly of free-standing nanostructures, a novel multifunctional platform for the continuous production of graphene and derivatives at the gram scale was developed. The platform is supported by a prototype plasma machine capable of performing a wide variety of industrially applicable processes within a single assembly environment. Free-standing graphene and nitrogen doped graphene, i.e., N-graphene nanosheets, and hybrid nanocomposites are assembled in a one-step process in seconds under atmospheric pressure conditions without the need of post-treatment. A single custom-designed machine enables the synthesis of an extensive array of hybrid nanomaterials featuring metal nanoparticles anchored in graphene. The method enables the conversion of a wide range of low-cost feedstock (e.g., ethanol, acetonitrile, etc.) into graphene and derivatives at a rate up to 30 mg/min. The resulting N-graphene sheets exhibit high quality, as evidenced by the highest reported presence of single atomic layers (45%), high ratio of 2D/G peak intensities in Raman spectra and N/O atomic ratio greater than one. The use of the obtained N-graphene in low secondary electron emission applications and in inkjet printing are explored. The presented plasma machine embodies significant potential to increase the effectiveness of plasma-driven process regarding productivity, costs and turnaround time.

1. Introduction

Considering the exceptional properties of graphene and graphene-based 2D materials and their entry into industry, it becomes extremely important to develop effective means to mass produce high-quality graphene and graphene-based hybrids. The extraordinary properties of graphene foster a multitude of prospective applications of graphene, including energy storage and conversion devices, sensors, nano-composites, photocatalysts, etc. [1,2]. Presently, the widespread market adoption is hindered by the relatively high cost, and the low quality of graphene and derivatives available on the marketplace [3,4]. Although the graphene market has grown, with about 250 companies currently

* Corresponding authors.
E-mail addresses: ines.vieitas@tecnico.ulisboa.pt (A. Dias), elena.stefanova@tecnico.ulisboa.pt (E. Tatarova).

https://doi.org/10.1016/j.apmt.2024.102056
Received 12 September 2023; Received in revised form 7 December 2023; Accepted 2 January 2024
Available online 20 January 2024

marketing graphene and derivatives in various forms, applications that rely on large-scale production have not experienced a take-off due to the very low quality of commercially available materials sold as graphene or graphene derivatives, as noted in Kauling et al. [4]. Notably, a recent study on the commercial graphene purchased from 60 companies worldwide has reported that the majority are selling a product containing less than 10 % graphene and that none of them supplied samples containing more than 50 % of graphene [4]. Research efforts face enormous challenges due to the lack of discernible protocols for producing customized graphene products and derivatives in ever-higher yields while maintaining their quality.

There are generally two approaches to fabricate carbon nanomaterials. The first one is known as “top-down” and consists in starting with a bulk material, i.e., graphite, and break it into smaller free-standing portions using mechanical, chemical, or other forms of energy. It is worth noting that for many applications (e.g. nanocomposites), the demand is often for graphene in the form of free-standing nanosheets since these, by contrast with their surface-supported counterparts, allow the utilization of both surfaces, effectively doubling the specific surface area and the associated surface processes performance. The top-down processes that have been reported include mechanical exfoliation of graphite, wet chemical reduction techniques that use graphite oxide, liquid-phase exfoliation, etc. [5–12]. The most used method for producing graphene sheets involves the chemical reduction of graphite oxide, known as the Hummers method [13]. Although cost-effective and suitable for large-scale production, this approach comes with significant drawbacks that affect the quality and performance of the resulting graphene. A notable concern is the use of toxic reducing agents, leading to environmental and safety issues. Furthermore, the method is extremely time-consuming, requiring hours of processing, and this extended duration not only increases operational costs, but also introduces inefficiencies into the production pipeline [1]. One of the critical limitations stems from the low electrical conductivity demonstrated by the materials obtained by Hummers’ method. This is due to the presence of unwanted residues, contamination, saturated sp^3 bonds and oxygen groups in the structure of graphene, which limit its potential applications. Recently, chemical- and solvent-free graphite exfoliation using plasma spraying has been reported [14]. Most notably, without using a solvent, synthesis rates of up to 48 g/h have been documented, with high level of repeatability. However, raw graphite materials from different suppliers, for example, have inconsistent morphologies and/or are contaminated with other residual constituents that can result in a wide distribution of quality and intrinsic properties [3,4]. These issues hinder the ability to tailor the properties of graphene for specific applications, and further treatment is required for customization.

The other strategy is designated by “bottom-up” and is based on the use of simple atomic or molecular species as "building blocks" to assemble nanostructures. The advantage of this ‘bottom-up nanotechnology’is the implementation of synthesis-by-design, through the control of the assembly process [15,16]. However, one of the most important problems is understanding/knowing how to promote specific molecular designs [15]. Currently, artificial manipulation of single atoms/radicals at the nanoscale seems dubious and almost impossible except through slow and laborious processes that render the technology industrially infeasible. Therefore, the natural way to implement synthesis by design is to create conditions that force the self-assembly of the atoms/radicals into the target nanostructure. The most representative example of bottom-up strategy is chemical vapor deposition (CVD) that involves growing graphene directly on a substrate by introducing carbon-containing gases, allowing better control over the growth conditions [17]. CVD allows the production of large area sheets (currently of interest for low power graphene-based electronics, sensors, optical devices), but its efficiency depends on the quality of the underlying polycrystalline metallic film (catalyst). CVD requires multiple processing steps to obtain transferable sheets and the resulting material is often contaminated with metal residues.

Furthermore, several examples regarding bottom-up approach synthesis of free-standing, i.e., substrate-free, carbon nanostructures via self-assembly process can be found in the literature [18–20]. Gravitational, electromagnetic fields, among others, can be used to create special conditions under which the self-assembly of a specific nanostructure takes place. To this end, the high-energy-density microwave plasma environment presents a unique 3D space for self-assembly of free-standing nanostructures enabling synthesis-by-design as demonstrated in [18–20].

Replacing C with N atoms affects the atomic charge distribution of graphene and creates “active sites” that increase the electrochemical activity of graphene, which greatly expands the range of applications. In nitrogen-doped graphene, denominated as N-graphene, nitrogen atoms incorporate the carbon lattice in any of three common bonding configurations, i.e., pyridinic, pyrrolic and graphitic. Quaternary nitrogen, i.e., N^+ ion with sp^3 hybridization can also be formed. However, despite of the numerous approaches available for N-graphene synthesis, either by direct or post-synthesis treatment, many issues remain unsolved. The direct CVD method, for instance, requires high temperature, vacuum systems and suffers from metal interference, low yield, and high cost [10,11,21,22]. Solvothermal approaches typically involve the mixing of lithium nitride with tetrachloromethane under moderate to high pressure and temperatures to facilitate the interaction of precursors during the synthesis [12]. It provides high yield and high doping levels, but with very high oxygen content. Graphene oxide (GO) and nitrogen precursors (e.g., urea, NH_3, etc.) are the initial materials for wet chemical methods and thermal treatment. The high temperature required for GO thermal treatment makes the process costly and inefficient. The wet chemical approaches can provide cost-efficient large--scale production but rely on the use of harsh chemistry and don’t provide control over the synthesis process [11,12,23].

It is worth noting that despite recent advancements [14] in graphene manufacturing, existing synthesis techniques remain in a nascent stage, characterized by high costs and a distinct lack of customization capabilities. The prevalent chemical methods entail numerous time-consuming and labor-intensive synthesis stages, often utilizing hazardous substances, leading to low quality material. As a result, there is a dedicated effort to explore innovative synthesis pathways that specifically address these pressing shortcomings and enable a higher quality graphene synthesis. The recently reported "flash graphene" fabrication method, for example, while having demonstrated potential to produce gram-scale quantities, can only use conductive solid carbons as a starting material and it is further limited by its intrinsic batch processing nature, its proneness to contaminate the product with material from the electrodes and the need for post-treatment [14,24]. Additionally, microplasmas, with their microscale dimensions and distinctive high-energy-density, along with a nonequilibrium reactive environment, stand out as promising tools for assembling advanced nanocarbons. A series of publications [25–27] have demonstrated innovative microplasma-enabled pathways for the controlled synthesis of graphene and its derivatives. These pathways showcase a catalyst-free and essentially continuous synthesis process, providing a significant contribution towards mass production of graphene.

Furthermore, remarkable progress can be made by using graphene as a matrix on to which nanoparticles are embedded. These hybrid materials offer significantly improved and varied properties due the synergy between graphene’s unique properties, such as high electrical conductivity [19], superior mechanical, thermal and chemical strength, tunable surface properties and resilience to high temperatures and aggressive chemicals, with properties of metal oxides (MO), resulting in new functionalities and properties. Significant synergetic effects occur in Graphene/Metal oxides (MO) hybrids due to the size effects and interfacial interaction [28]. In addition, MO nanoparticles attached or anchored on graphene sheets suppress agglomeration by serving as nano-spacers and, as a result, increase the accessible surface area

[29–31]. Moreover, graphene acts as a highly conductive matrix, which can improve the electrical properties and charge transfer channels of pure oxides. Numerous nanoarchitectures of graphene/metal oxides with varieties of MO (Mn_3O_4, MnO_2, Fe_2O_3, Fe_3O_4, etc.) have been proposed [28–32]. Besides, nitrogen incorporation can strengthen the binding forces between metal nanoparticles and graphene matrix due to the N-induced modification of the surface charge distribution on the scaffold, with active charge sites available for nanoparticles anchoring [33–35]. The transition metal chalcogenides (TMCs), such as MnS and MnS_2, exhibit high electrical conductivity over the corresponding transition metal oxides but unsatisfactory electrochemical performance. Thus, the synthesis of N-graphene-MO (NGMO) and N-graphene-MS (NGMS) hybrid nanostructures constitute an effective approach to the creation of nanomaterials with excellent electrochemical performance. So far, the main synthesis strategies for graphene/N-graphene metal oxides/sulphides hybrids include chemically based methods [32,36-42] such as sol-gel [43–47], hydrothermal/solvothermal [48–52], self-assembly [53], microwave irradiation [54–59]. However, the use of hazardous chemicals leads to deterioration of the properties of the nanostructures.

To this end, given the synergistic thermal, chemical, and catalytic properties of microwave plasmas, plasma-based methods represent a highly competitive, sustainable, and environmentally friendly route for the bottom-up synthesis and engineering of nanocarbons. So far, plasmas have been used to synthesize numerous nanostructures, like graphene nanowalls, nanotubes, nanowires, etc. [20], as well as free-standing graphene sheets and derivatives [19], the latter often required in different applications. As demonstrated in recent patents and articles [18-20,60-64], the exclusive plasma mechanisms to master the quanta and localization of energy and matter at atomic scale levels leads to effective control of the material quality. The plasma-driven self--assembly of graphene begins with the formation of "building blocks" (C atoms, C_2 radicals, etc.) in the "hot" plasma zones and the formation of carbon nuclei in the "colder" ones. The self-assembly process requires very rapid delivery of the "building units" and equally rapid supply of energy to overcome any actual potential barriers for growth of the nanostructures. In other words, the “building units” and energy flows must be tuned to force the self-assembly of planar hexagonal lattice nanostructures [18,19].

Here, we present a novel versatile platform for continuous gram-scale production of graphene and derivatives based on a microwave plasma machine prototype. This unique machine provides a wide variety of industrially applicable plasma-driven processes that allow the synthesis-by-design of complex 2D nanocarbons to be performed within a single assembly environment. Free-standing graphene/N-graphene sheets and an extensive array of graphene-based hybrids are assembled by a one-step streamlined process in a matter of seconds, under atmospheric pressure conditions, without the need for chemicals nor cleaning, washing or other post-treatment operations. Hybrid nanomaterials feature graphene/N-graphene as a highly conductive matrix where metal (MnO_2, Fe_2O_3, oxy-MnS) nanoparticles are anchored.

The used plasma approach enables the conversion of a wide range of low-cost precursors (e.g., ethanol, methane, acetonitrile) into graphene and derivatives at a high production rate (up to 30 mg/min). Besides, it enables reduction of micrometer-sized metal particles to nanoparticles and conversion into different chemical phases. The complex plasma environment was tailored to ensure selective, i.e., predominantly one carbon allotrope, synthesis. Thanks to plasma properties, the developed technology ensures an effective and reproducible control, at atomic scale level, over the fluxes of energy and matter towards the growing nanostructures, which results in reproducible synthesis with predefined outcomes and very high selectivity regarding single atomic layers. The microwave plasma-driven chemicals-free self-assembly process circumvents drawbacks associated with chemical methods. Produced N-graphene sheets exhibit high quality as evidenced by the highest reported presence of single atomic layers (45%), high ratio of 2D/G peak intensities in Raman spectra and N/O atomic ratio greater than one, indicating a well-preserved hexagonal lattice structure of graphene. The key advantage of the method lies in the ability to finely adjust the density and energy of the primary "building units," such as C_2 radicals, C, and N atoms, within the high energy-density plasma environment. This precise tuning empowers effective control over the energy and material fluxes directed toward the growing nanostructures in the reactor’s assembly zone and ensures rigorous control over the synthesis process. Moreover, the same plasma-based machine can be used to assemble different graphene derivatives and hybrids by changing the synthesis protocols. Table S1 and S2 (SI) present a comparative analysis of the present method for N-graphene and hybrids synthesis with the previously used methodologies. Benefiting from the unique and exquisite properties of the produced material (e.g., graphene, N-graphene) prospective applications are demonstrated.

2. Experimental

2.1. Nanomaterials synthesis

A schematic representation of the plasma-based synthesis process is shown in Fig. 1, while a more detailed description of the prototype is given in the SI (Fig. S1). A waveguide surfatron-based setup [65] is used to create a surface wave (SW) induced microwave plasma at atmospheric pressure conditions. The SW sustained discharge is produced by the field of a travelling wave (represented by the red lines in Fig. 1) that simultaneously propagates and creates its own propagation structure, sustaining the plasma along an extended active zone outside the wave launcher. In this way, large microwave power-densities can be injected into the processing area and high densities of relevant active species can be achieved. The discharge takes place inside a quartz tube with expanding radius, inserted perpendicularly to the waveguide wider wall and directed downstream. The design permits controlling the thermodynamic conditions (gas velocity, thermal fluxes, residence time, etc.) in the plasma reactor. The residence time can be controlled via the gas flow of matrix Ar gas, under laminar conditions.

The plasma reactor possesses two distinguishable zones: a "hot" zone, sustained by surface waves and an afterglow "mild" plasma zone (Fig. 1). In the former, carbon/nitrogen precursors are introduced alongside a background flow of argon (Ar) under laminar or vortex conditions. Electrons absorb the wave power and consequently transfer it via elastic and non-elastic collisions to heavy particles and gas temperatures up to 4000 K can be achieved (Fig. S2). Consequently, the injected carbonaceous molecules are decomposed into the fundamental components of carbon nanostructures, namely carbon atoms and C_2 radicals. Subsequently, the newly formed carbon atoms and C_2 molecules are transported by the Ar gas flow towards the "mild" afterglow zone, characterized by lower gas temperatures ranging from 2000 K to 500 K. Upon passing through a designated “vaporization surface”, an isothermal plasma surface with a temperature of approximately 2500 K (Fig. 1), gas-phase carbon atoms and C_2 molecules undergo a transformation into solid nuclei. This transition occurs within the larger volume of the "mild" zone, where kinetically-driven processes of assembly and growth of free-standing flowing carbon nanostructures take place [19]. Using a reactor with an expanding radius allows: i) larger power densities inside the smaller radii sections, and consequently larger fluxes of “building units”, i.e., C_2 and C atoms, with sufficiently high energy towards the assembly plasma zone; ii) deliberately create conditions that promote the departure from supersaturation environment in the larger radii, larger volume "mild" zone. In the latter, the density of carbon nuclei decreases, creating favorable conditions for the formation of planar nanostructures. Moreover, the assembling process requires a very fast delivery and stacking of the “building units” and an equally fast supply of enough energy to overcome all the actual potential barriers, and a well-tuned residence time of the levitating growing nanostructures.

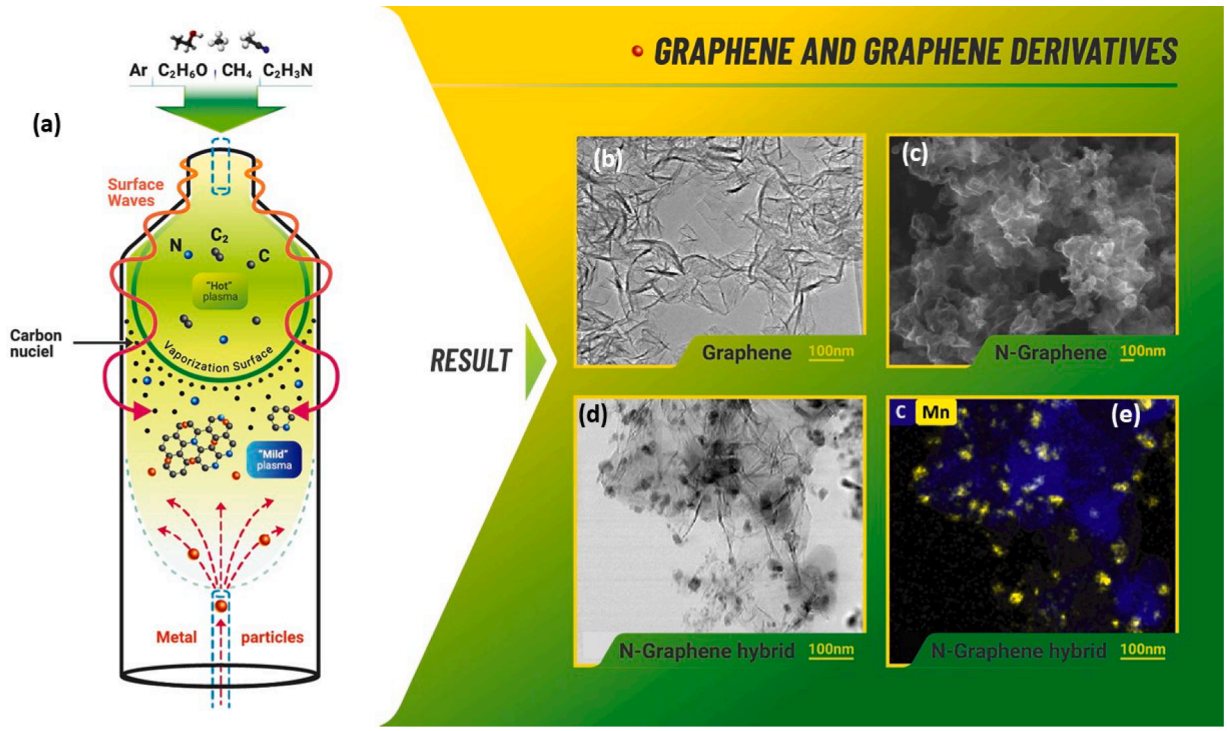

Fig. 1. a) Schematic representation of the plasma reactor used for the production of free-standing graphene nanosheets and hybrid nanostructures. b) Transmission Electron Microscopy (TEM) micrograph of a graphene sample. c) Scanning Electron Microscopy (SEM) image of N-graphene sample. d) Scanning Transmission Electron Microscopy-high-angle annular bright field (STEM-HAABF) image of the manganese oxide-graphene (MnOG) hybrid and corresponding e) Energy Dispersive X-ray (EDS) mapping of the elemental distribution.

It must be noted that the synthesis of selected nanostructures with specific structural quality is the result of a synergistic fine-tuning of the "hot" plasma environment and thermodynamic conditions in the "mild" zone. Operational parameters, including background gas and precursor partial fluxes, are meticulously adjusted to meet the pre-requisites, i.e., to promote the self-assembly of planar sp^2 structures in the "assembly" zone of the plasma reactor. In essence, the engineered interplay of kinetic and thermodynamic factors allows for precise control over the nucleation and growth processes, paving the way for the tailored synthesis of graphene nanosheets.

Furthermore, to achieve a controlled in situ N-doping, two different approaches, i.e., top-down and bottom-up, were used to introduce nitrogen precursors into the plasma reactor (Fig. S1a). The top-down configuration provides injection of both the carbon and the nitrogen precursors mixed with argon gas (Q_{Ar}') into the "hot" plasma zone. Acetonitrile injected from top in the "hot" plasma zone, for example, was used both as a carbon and nitrogen precursor. Considering the bottom-up approach, only carbon precursor is injected from the top, while nitrogen precursor mixed with argon (Q_{Ar}'') is sprayed into the "mild" plasma zone against the main flux (see Fig. 1, in SI Fig. S1 and S3).

The plasma environment was deliberately tailored to achieve selective synthesis, specifically targeting one predominant carbon allotrope, i.e., graphene nanosheets. The choice of selected plasma reactor geometry and carbon precursors are crucial to ensure the exclusive synthesis of graphene nanosheets within a narrow range of operational parameters, encompassing microwave power, background gas flux, and precursor fluxes. The optimization of these conditions for the selective synthesis of graphene/N-graphene involves a meticulous exploration to pinpoint the parameters that maximize the 2D-to-G band ratio in the corresponding Raman spectrum, which constitutes a good metric for determining the preservation of the materials' desired properties.

Diverse protocols for selective synthesis have been established, each tailored to distinct carbon and nitrogen precursors. These protocols serve as structured methodologies, ensuring reproducible outcomes in terms of production rate, structural quality (including aspects such as the presence of sp^3 carbons, lateral dimensions etc.), and chemical composition (such as the presence of oxygen). The establishment of these protocols provides a roadmap for achieving targeted results with a high level of reproducibility, thus offering a level of predictability and control over the synthesis process.

In order to synthesize nanocomposites, simultaneously with the generation of graphene/N-graphene sheets, a controlled flow of micron-sized particles (MnO_2 or oxy-MnS, Fe_2O_3) is injected upstream at a specific position in the "mild" plasma zone. The particles rapidly heat up to the temperature of the background gas, which is around 2000 K in this zone. Due to the plasma's thermal and chemical reactor functions, the micron-sized particles undergo plasma-enabled size reduction and are converted to nanoparticles. Besides, due to the chemical reactions with radicals and molecules (H_2, O_2, CN, HCN, etc.; Fig. S3) different chemical phases are created and the nanoparticles are attached and/or anchored to the growing graphene/N-graphene sheets. Hundreds of milligrams of ready-to-use free-standing graphene/N-graphene sheets and graphene-based hybrids can be fabricated in minutes. In order to preserve graphene/N-graphene properties, protocols for synthesis of hybrid structures have been established targeting the maximization of the 2D/G ratio in the Raman spectra of the produced samples.

2.2. *Characterization techniques*

Transmission Electron Microscopy (TEM, JEOL JEM-2010F, operating at 200 kV) was used to study the samples morphology. Scanning Transmission Electron Microscopy (STEM, DCOR Cs probe-corrected FEI Titan G2 60–300 instrument) combined with a Super-X energy dispersive X-ray spectroscopy (EDS, Bruker) were used to perform high-angle annular dark field (HAADF), bright-field (BF) and elemental mapping analysis. Raman spectra were taken from different regions of the samples (LabRAM HR Visible, Horiba Jobin-Yvon at 633 nm and laser power of 0.054 mW). X-ray diffraction analysis (XRD) was performed using a

Bruker D2 Phaser diffractometer, equipped with a CuKα source (λ=0.154184 nm). X-ray Photoelectron Spectroscopy (XPS, KRATOS XSAM800 spectrometer with a double anode Mg/Al, operating in Fixed Analyzer Transmission mode, with a pass energy of 20 eV and non-monochromatic Mg Kα X-radiation - 1253.6 eV, produced with a power of 120 W) and Near Edge X-ray Absorption Fine-Structure (NEXAFS, HE-SGM beam line at BESSY II storage ring, data collected in Partial Electron Yield mode) have been used to provide chemical analysis of the produced nanostructures. Detailed information is provided in Supplementary Information.

3. Results and discussion

3.1. Free standing graphene sheets

Aiming at the synthesis of pure graphene nanosheets, ethanol and methane have been used as carbon precursors. Following the established protocols, selective synthesis of free-standing graphene nanosheets have been achieved. As seen from Fig. 2a the morphology of the synthesized structures is typical for free-standing graphene, i.e., disordered sheets entangling each other. The individual nanosheets can be easily distinguished - the darker areas in the image correspond to regions with wrinkles, folding and overlapping of the sheets. The corresponding Raman spectra, collected from different locations of the sample, contain the three main features of graphene-like structures, namely D, G and 2D peaks [19]. The G peak is a primary in-plane vibrational mode, common to all sp^2 carbon systems. The D-band, so-called 'disorder' band, appears due to structural disorder, the presence of sp^3 carbon and dangling bonds at the flake edges. The fingerprint of graphene in the Raman spectra, i.e., the 2D band activated by a second order scattering process, provides evidence that the carbon nanosheets obtained are indeed graphene (Fig. 2d). The XRD pattern (Fig. 2e) of the graphene sample contains the main line at 2θ ~ 25.84° corresponding to Miller index (002), which results from the interference between two planes in graphite. The estimated interlayer distance is ~ 3.45 Å, significantly larger than the 3.35 Å found in graphite, indicating the expanded and turbostatic structure of graphene sheets [66]. The lateral size of the flakes is in the range 100–1000 nm, with a minor fraction at 5000 nm (Fig. 2f). The achieved production rate was 10 mg/min. The chemical composition of the graphene sample considered revealed 98.5 *at.*%C and 1.5 *at.*%O (Fig. 2b, c). High sp^2 carbons ~68 % and very low oxygen impurity additionally confirm the high quality of the synthesized graphene.

3.2. Free-standing N-graphene sheets

To synthesize nitrogen-doped graphene, i.e., N-graphene, applying a top-down approach, acetonitrile is used as both a carbon and a nitrogen precursor. The acetonitrile, delivered in the "hot" plasma zone, decomposes completely due to the collisions ($CH_3CN \rightarrow H + CH_2CN$, $H + CH_3CN \rightarrow HCN + CH_3$, $CH_3 + CH_3CN \rightarrow CH_4 + CH_2CN$), leading to the formation of active radicals: H, CH_3, HCN, etc. (Figs. S3, S5). The HCN molecule is considered as the main "building block" of N-graphene. A typical transmission electron microscopy image of the produced nanostructures is shown in (Fig. 3a). It reveals the common graphene-like morphology, i.e., a well-established thin curled paper-like structure, where the percentage of monolayers is ~ 46% (Fig. 3b). The sample also contains bi-layer, tri-layer and higher-order multilayer sheets. All Raman spectra collected from different locations of the sample reveal a well-pronounced and intense 2D peak, demonstrating that few-layered graphene-like sheets were produced (Fig. 3c). The D/G ratio in the different spectra is nearly constant, indicating homogeneous doping. The graphitic (002) X-ray diffraction (XRD) peak occurs at a diffraction angle 2θ ~ 25.84 ° (Fig. 3d). The estimated interlayer distance is 3.44 Å. The lateral size of the N-graphene flakes is in the range 100–1000 nm (Fig. 3e). The production rate of N-graphene sheets is ~ 30 mg/min.

Carbon, nitrogen and oxygen were identified in the survey spectrum, obtained by X-ray photoelectron spectroscopy (XPS) (Fig. S5). The XPS results demonstrate that N-graphene with a high doping level of ~ 2.8 *at.% N* and relatively low oxygen impurity (~ 2.2 *at.% O*) was synthesized. The good structural quality is evidenced by the high relative amount of sp^2 carbon ~67 %. Multilayer N-graphene with high production rate (30 mg/min) was also synthesized by applying the bottom-up approach (Fig. S6).

3.3. Graphene/N-graphene-based hybrids

3.3.1. Graphene/N-graphene-based hybrids synthesized under laminar flow of background inert gas

To synthesize N-graphene-manganese oxide hybrids, methane and

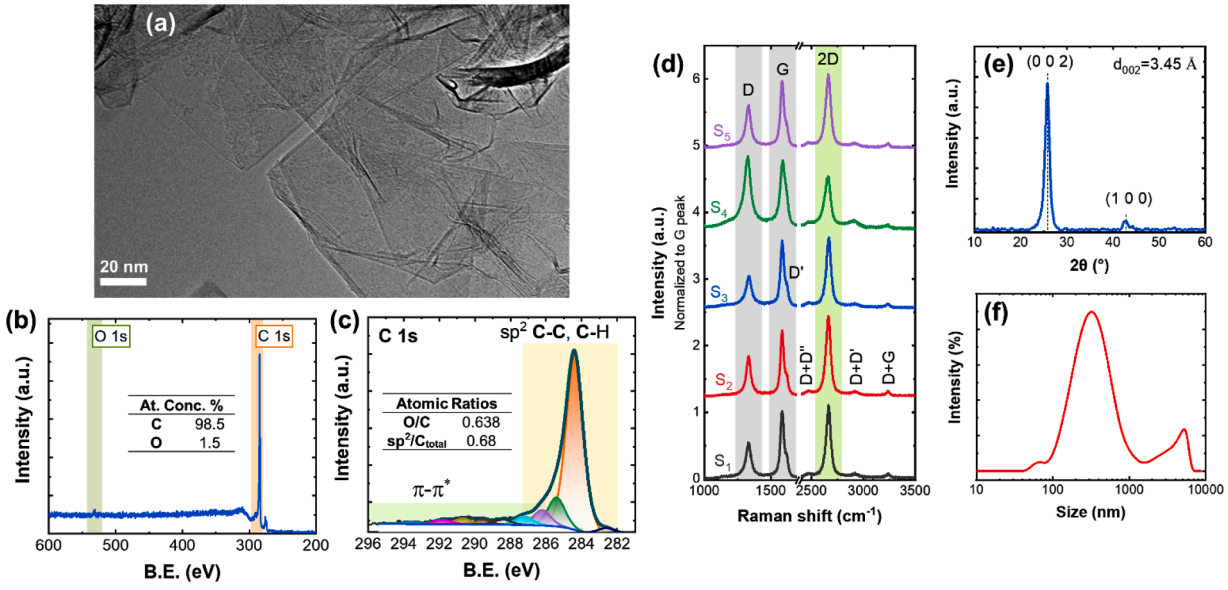

Fig. 2. a) TEM images of graphene nanosheets produced with ethanol. b) XPS pattern, c) close-up of the XPS pattern in the C 1 s region of graphene and corresponding chemical composition analysis. d) Raman spectra collected from different locations of the sample. e) XRD pattern of graphene nanosheets. f) Size distribution of the sheets (Zetasizer Nano). Experimental conditions: $Q_{Ar} = 6$ slm, $Q_{Ar'} = 3$ slm, $Q_{Eth/Ar} = 600$ sccm, $T_{Eth} = 45$ °C, $P = 6$ kW).

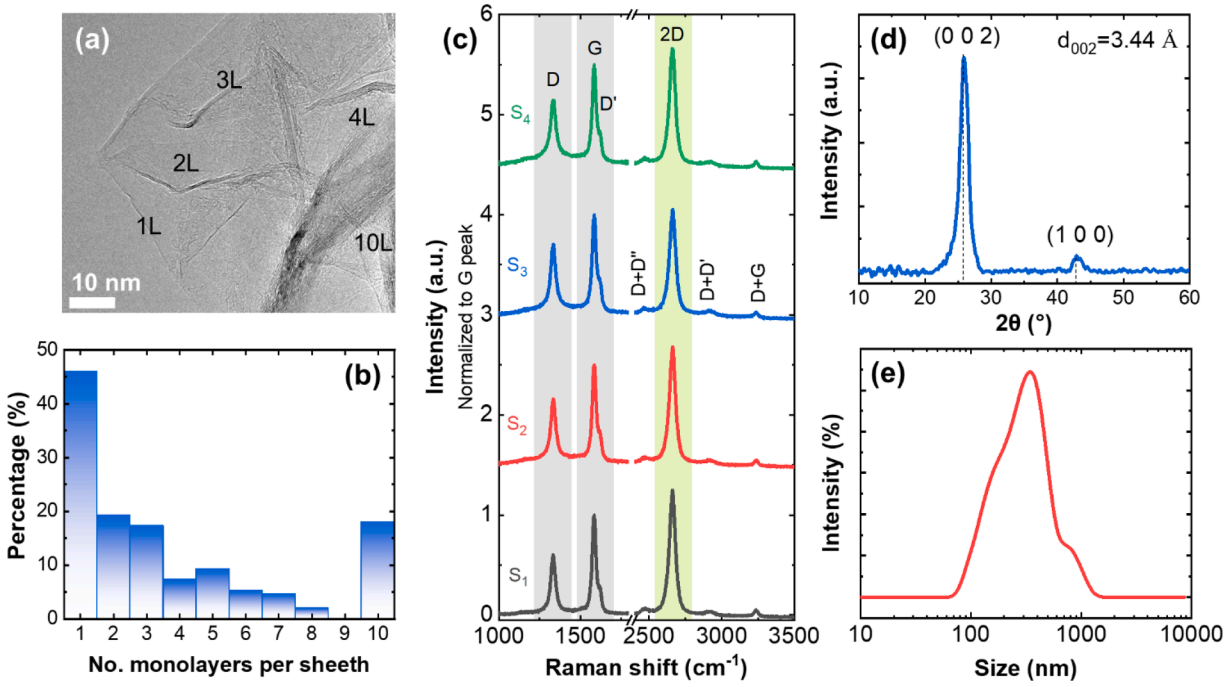

Fig. 3. a) TEM image of free-standing N-graphene sheets produced using acetonitrile as a precursor. b) Number of monolayers per sheet estimated from HRTEM images' analysis. c) Raman spectra collected from different randomly selected locations in the N-graphene sample. d) X-ray diffraction (XRD) pattern of the N-graphene sample. e) size distribution of the sheets evaluated by dynamic light-scattering analysis. Experimental conditions: $Q_{Ar} = 5.4$ slm, $Q_{Ar'} = 3$ slm, $Q_{Ar/Acet} = 400$ sccm, $T_{Acet} = 45$ °C, $P = 6$ kW).

methylamine, as carbon and nitrogen precursors, were injected into the "hot" plasma zone. Simultaneously, a controlled jet of manganese-dioxide (MnO_2) micrometer-sized particles was sprayed into the plasma afterglow region. The Scanning Transmission Electron Microscope - high-angle annular bright field (STEM-HAABF) image and Energy Dispersive X-ray Spectroscopy (EDS) mapping show well-distributed oxidized manganese nanoparticles in the hybrid nanostructure (Fig. 4a-d).

The nanocomposite comprises transparent paper-like structures and metal nanoparticles. The Raman spectra (Fig. 5a), obtained from three random spots, exhibit intense and sharp 2D peaks. The intensity ratio between the G and 2D peaks is ~0.7 and the FWHM of the 2D peak is ~ 25 cm^{-1}, indicating the presence of a few layers in the N-graphene sheets of the hybrid. The spectra detected from the random locations in the sample are different, implying an expectable inhomogeneity, since nanoparticles are attached to and between the sheets. This result agrees with STEM observations. The XRD analysis confirms the dominant presence of cubic Fm3m MnO phase (PDF#07–0230, $a = 0.4445$ nm). Other minor diffraction peaks, assigned to Mn (PDF 21–0547) and tetragonal I41/and α-Mn_3O_4 phases (PDF #24–0734, $a = 0.5762$ nm), are observed as well (Fig. 5d).

The doping of graphene with nitrogen and the anchorage with manganese oxide nanoparticles (<30 nm, see Fig. 5g) is attested by the detected C 1 s, N 1 s, O 1 s and Mn 2p lines, observed in the XPS survey spectrum in Fig. 5h. Although the XPS N 1 s region shows that nitrogen is mainly from a mixture of pyridinic and pyrrolic configurations, and probably also from some amide groups (fitted peaks centred at 398. 6 ± 0.1 eV and 399.9 ± 0.1 eV), it is relevant to highlight the peak centred at 397.3 ± 0.1 eV, which is assigned to nitrogen bonded to manganese (Fig. 5i). Mn 2p is a doublet with spin-orbit split of energy, but only the main component of the doublet is shown in Mn $2p_{3/2}$ region (Fig. 5k), the main fitted peak is centred at 641.5 ± 0.1 eV, that is a slightly lower binding energy (BE) than that predicted for Mn^{4+} in MnO_2 (which was the metal oxide used as precursor). This attests the reduction of Mn^{4+} to Mn^{2+} or Mn^{3+} during the plasma synthesis. The O 1 s region (Fig. 5j) was fitted considering four peaks centred at 529.6 ± 0.1 eV and 531.3 ± 0.1 eV, assigned respectively to metal oxide and hydroxides, 532.7 ± 0.1 eV which includes oxygen atoms bonded to carbon, and 534.6 ± 0.1 eV from occluded water (Table S3). The production rate of #MnONG hybrid under conditions considered is ~ 15 mg/min.

To synthesize N-graphene-manganese sulphide hybrids, methane and methylamine were injected into the "hot" plasma region, along with a controlled stream of oxy-manganese-sulphide (MnS*) microparticles sprayed in the plasma afterglow region. STEM-HAADF images and the corresponding EDS analysis show dispersed metal sulphide nanoparticles on the well-defined transparent graphene sheets (Fig. 4e-h). The well-preserved graphene structure is also confirmed by Raman spectra (Fig. 5b). TEM images of the N-graphene-manganese sulphide hybrid (Fig. S8) show encapsulated squared nanoparticles (~30 nm size); in this case the nanoparticles behave not only as spacers as seen in the STEM image, but also as catalysts. The XRD pattern (Fig. 5e) evidences two main phases in the sample, MnO (PDF 7–0230) and MnS (PDF 40–1288). N-graphene peak at 26.6 ° is also well manifested. XPS analysis shows in detail the different sulphur-based species anchored in N-graphene sheets (Fig. S8, Table S4). The production rate of #MnSNG hybrid under the conditions considered is ~ 15 mg/min.

Considering the synthesis of graphene-iron oxide hybrids, methane was used as carbon precursor and micrometre-sized iron oxide (Fe_2O_3) particles were injected into the afterglow region. The STEM-HAABF image and the EDS element distribution maps (Fig. 4i-l) show the agglomeration of structures at different degrees of crystallinity. Fig. 4i shows folded and entangled thin wavy sheets, seen as transparent zones with dark lines due to the folding up of the sheet edges. The EDS analysis indicates the presence of iron nanoparticles, well dispersed in the matrix of graphene sheets. The EDS maps of carbon and oxygen reveal the presence of graphene oxide structures since the image is practically the same for both elements. Furthermore, while comparing the EDS maps of oxygen and iron, it is possible to identify the presence of pristine iron nanoparticles with possible/residual presence of oxidized iron nanoparticles. The XRD analysis shows the typical for graphene peak at 2θ~26 ° (Fig. 5f). The dominant peaks are attributed to the α-Fe phase (PDF 06–0696). Other peaks observed are assigned to γ-Fe (PDF

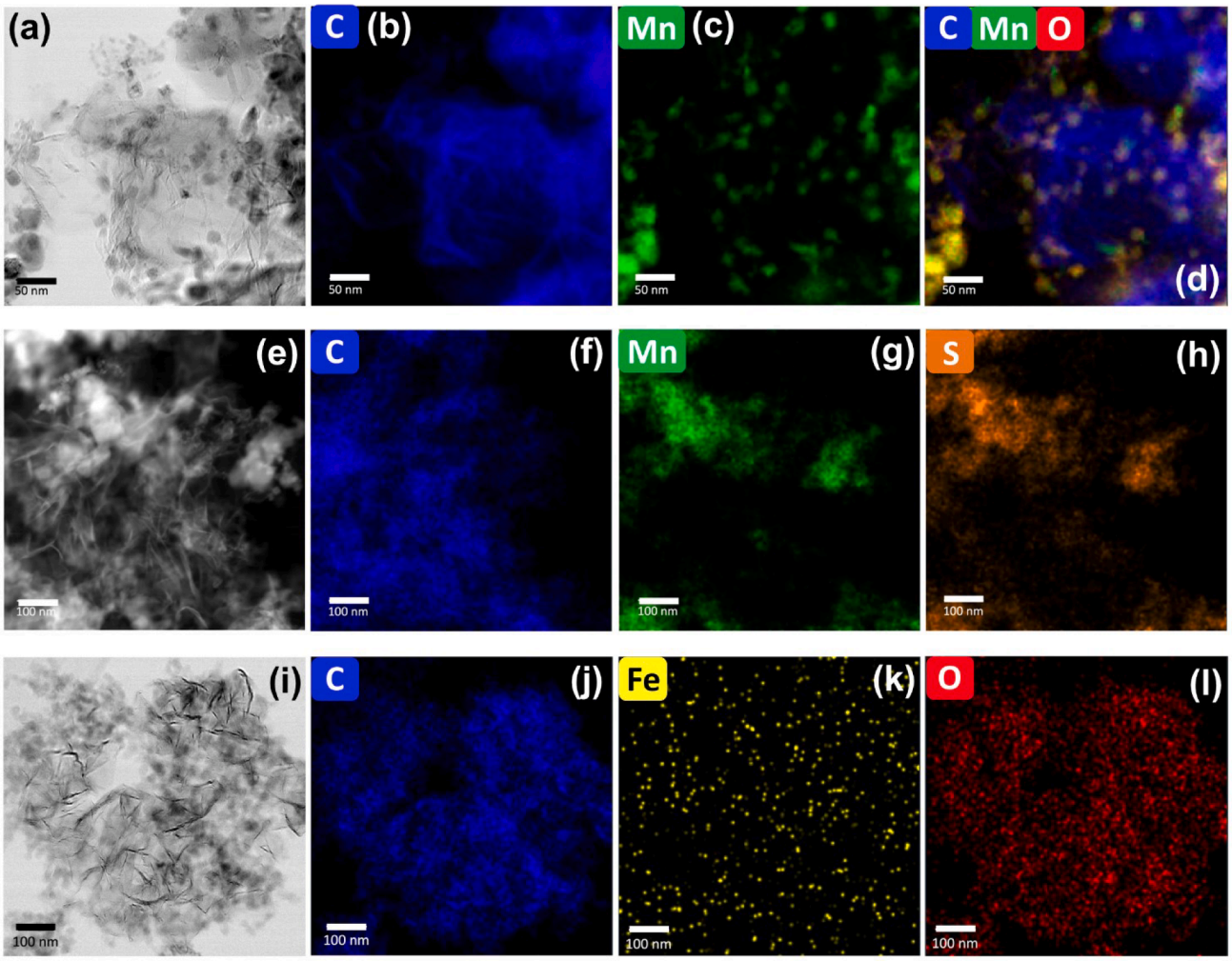

Fig. 4. (a, e, i) STEM images of the MnONG, MnSNG and FeOG hybrids, respectively, and corresponding (b-d, f-h, j-l) EDS element distribution maps. Images scale: (a-d) 50 nm; (e-l) 100 nm. Experimental conditions for #MnONG: Q_{Ar}=5.4 l/m; $Q_{Ar''}$=2.07 l/m; Q_{CH4}=80 sccm; Q_{CH3NH2}=20 sccm; $Q_{Ar\ through\ MnO2}$=500 sccm; P = 3.3 kW. Experimental conditions for #MnSNG: Q_{Ar}=5.4 l/m; $Q_{Ar''}$=2.07 l/m; Q_{CH4}=80 sccm; Q_{CH3NH2}=20 sccm; $Q_{Ar\ through\ MnS^x}$=500 sccm; P = 3.9 kW. Experimental conditions for #FeOG: Q_{Ar}=9.4 l/m; $Q_{Ar''}$=3 l/m; Q_{CH4}=130 sccm; $Q_{Ar\ through\ Fe2O3}$=200 sccm; P = 4.86 kW.

31–0619), γ-Fe_2O_3 (PDF 25–1402) and Fe_3O_4 (PDF 19–0629), which is in accordance with the STEM and EDS analyses. The Raman spectra of three randomly chosen spots of the graphene-iron oxide hybrid shows a homogeneous sample, containing multi-layered graphene sheets (Fig. 5c). Results from XPS and NEXAFS analyses (Fig. S9) support these conclusions. The production rate of #FeOG hybrid under the conditions considered is ~ 25 mg/min.

3.3.2. *N-graphene-based hybrids synthesis under vortex flow of background argon gas*

To improve the quality of synthesized N-graphene/MnO hybrids and to achieve homogeneous distribution of MO nanoparticles vortex flow of the background Ar gas under swirl injection of the later was employed. For the N-graphene nanosheets synthesis acetonitrile was used as both carbon and nitrogen precursor. Simultaneously, a controlled jet of manganese-dioxide (MnO_2) micro-particles was sprayed into the plasma afterglow region.

The TEM analysis, STEM image and respective EDS of N-graphene metal-oxide composites (NGMOs) indicate the presence of well-dispersed nanoparticles in the matrix of N-graphene sheets (Fig. 6a-e).

The nanoparticles with nearly spherical morphology and size <30 nm are homogeneously distributed over the graphene sheets (Fig. 6a-e, h). Positioning the injection point closer to the hot plasma zone (18 cm from the launcher), favours the synthesis of two phases, namely MnO (PDF 07–0230) and Mn (PDF 21–0547), see Fig. 6g. This is confirmed by the corresponding NEXAFS analysis made (see SI Fig. S10). This is in contrast with laminar flow condition for the Ar matrix gas, where three different phases are present (see Fig. 5d). The Raman spectra, obtained from five different randomly chosen spots of the NGMO sample, are shown in Fig. 6f. The three main peaks, attributed to D, G, and 2D-bands typical for the graphene-like materials are present, although there are regions with a low intensity 2D peak. The inhomogeneity of the samples is expected, since nanoparticles are attached to and between the sheets. This result is in accordance with HRTEM and STEM observations (Fig. 6a-c). The intensity ratio between the 2D and G peaks and the full width at half maximum (FWHM) of the 2D peak indicates that multi-layered graphene sheets are present in the NGMO hybrids. The intensity of D and D' (small shoulder of G) peaks is intrinsically related with defects, i.e., type of defects and respective concentration in the graphitic structure. Therefore, the D band intensity of the spectra evidences the nanoparticles presence and the nitrogen doping of the graphene sheets.

3.4. *Applications*

The quality of the N-graphene synthetized in this work was compared to that of a commercially available product, obtained from a reference supplier (Fig. 7b). The most distinctive difference is observed

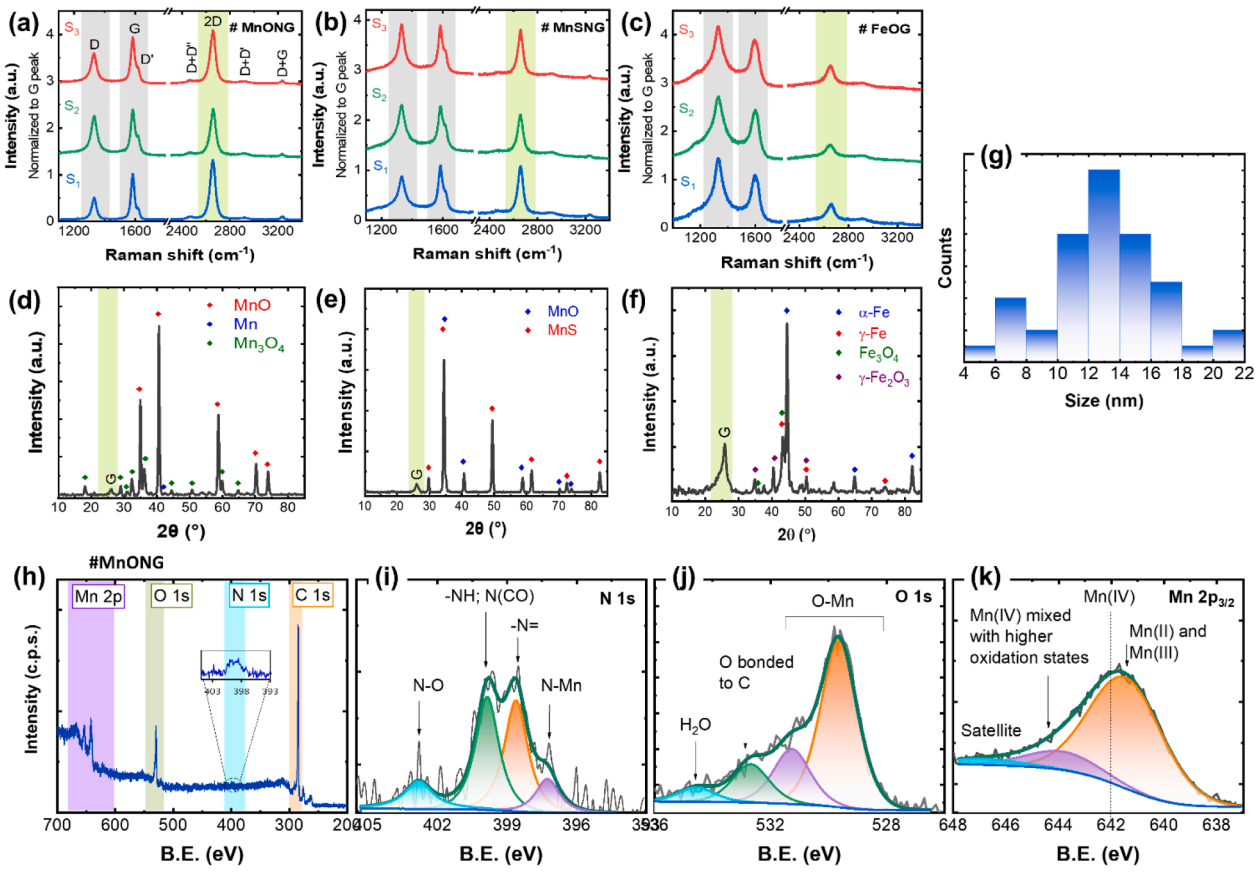

Fig. 5. a-c) Raman spectra taken from three randomly chosen spots of the #MnONG, #MnSNG and #FeOG hybrids, respectively; and corresponding (d-f) XRD pattern. g) size distribution of the nanoparticles and (h-k) XPS analysis of the N-graphene/oxide-manganese (#MnONG) hybrid. h) Survey XPS spectrum, i) N 1 s, j) O 1 s and k) Mn $2p^{3/2}$ XPS regions. Experimental conditions for #MnOG, #MnSG and #FeOG samples: same as in Fig. 3.

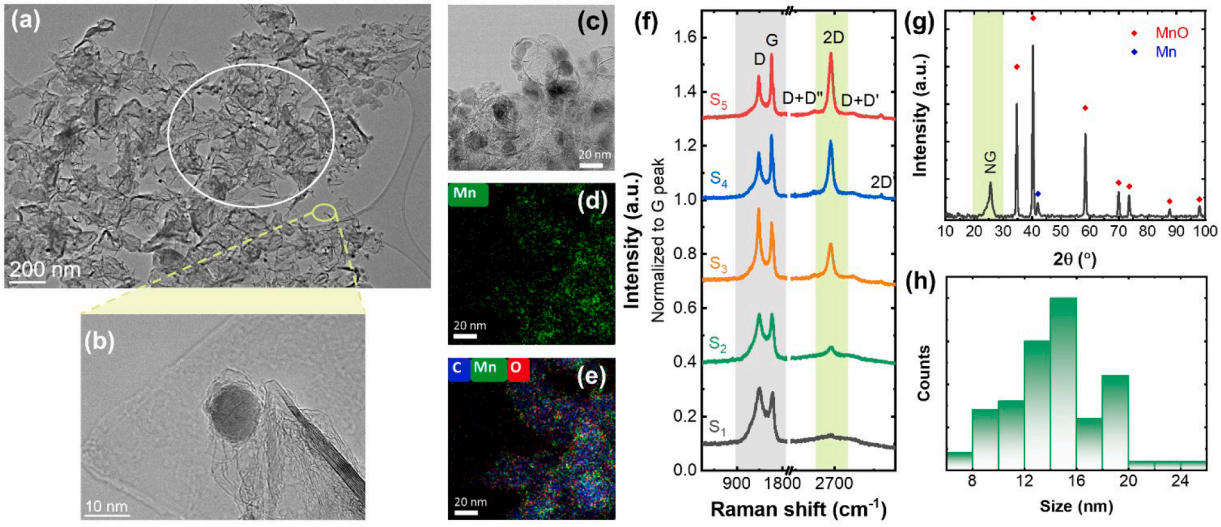

Fig. 6. a) TEM images of N-graphene/MnO hybrid produced with acetonitrile, b) magnified image of the region encircled in yellow in a). c) STEM image of NGMO hybrid. d,e) EDS element distribution map; f) Raman spectra collected from randomly selected locations in the N-graphene sample. g) X-ray diffraction (XRD) pattern. h) size distribution of nanoparticles of N-Graphene/MnO hybrid. Experimental conditions: Q_{Ar}= 7.4 l/m; $Q_{C_2H_3N}$ = 90 sccm; $T_{C_2H_3N}$ = 45 °C; $Q_{Ar\ through\ MnO_2}$=200 sccm; $Z_{inj\ MnO_2}$=18 cm; P = 5.4 kW.

between the two Raman spectra (Fig. 7a), where the 2D-band (the fingerprint of graphene) is missing in the commercial carbon product. In the spectrum of synthesized N-graphene, a narrow, high-intensity and well-pronounced 2D-peak is present, demonstrating that even at relatively high level of doping (e.g., ~2.8 at% N) the graphene structure is well preserved. The overview of the current situation regarding different methods for N-graphene synthesis and the quality of the synthesized material is shown in Fig. 7c. As seen, the N-graphene produced in the present work presents higher quality when compared with the commercial material produced by currently used methods, evidenced by an

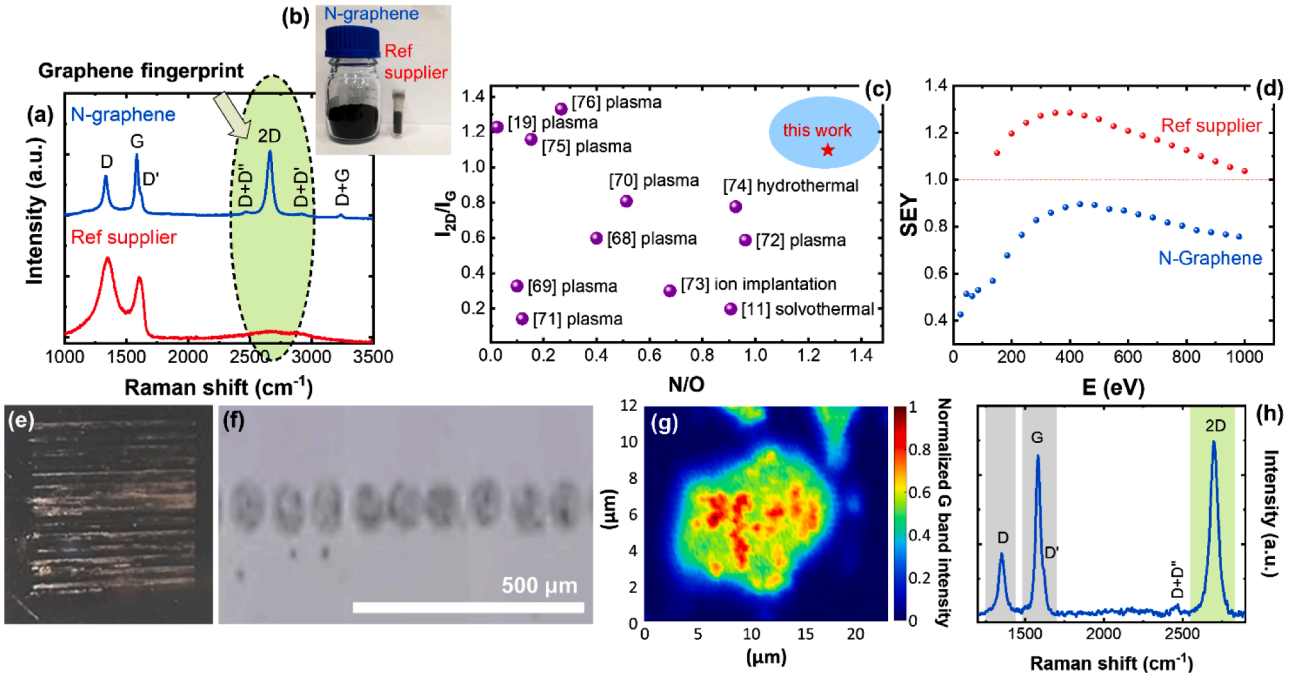

Fig. 7. a) Raman spectra of N-graphene synthesized in this work (with 2.8 at%N) and of the sample obtained from a reference supplier. b) Photo of containers with 250 mg of N-graphene each, produced in this work and obtained from reference supplier. c) Current situation regarding different methods for N-graphene synthesis [11,19,68-76]. d) Plot of SEY vs energy for a sample of N-graphene produced in this work (blue dots) and for the "low SEY" material from a reference supplier (red dots). e) Optical micrograph of N-graphene printed on a silicon wafer. f) micrograph of a single line with distinguished points. g) Raman mapping of a single point. h) Average Raman spectrum taken from randomly chosen regions of printed N-graphene lines. Experimental conditions: Q_{Ar} = 5.4 slm, $Q_{Ar'}$ = 3 slm, $Q_{Ar/Acet}$= 600 sccm, T_{Eth} = 45 °C, P = 6 kW).

N/O atomic ratio greater than one and a high 2D/G peak intensity ratio in the Raman spectra.

The N-graphene produced by the plasma machine was also explored in secondary electron emission (SEE) experiments (see Supplementary Information for more detailed information). Low SEE materials have applications in different fields, including accelerators and space technologies. The Secondary Electron Yield (SEY) of the N-graphene sample synthesized in this work is below 1 (Fig. 7d). As established earlier, doping with nitrogen leads to changes in the electronic structure of the material with the suppression of graphene π-plasmons, which, together with the corrugated morphology, results in a decrease in the SEY [67]. The SEY values of N-graphene are about 1.45 times lower than those of a commercial reference supplier (see Fig. 7d).

An important aspect of possible applications of graphene concerns the printing of this material. Fig. 7e-f show the optical image of inkjet-printed drops of graphene on a silicon substrate. The structural organization and properties of the printed graphene structures were analyzed by Raman spectroscopy (Fig. 7e, f). The Raman spectra (Fig. 7g, h) display the characteristic features of graphene with four prominent features. The D and G peaks confirm the structural defects and the graphitic nature of the materials. The D' band corresponds to phonons near the Brillouin zone centre and indicates the surface defects and edge effects. Also, the presence of a dominant 2D peak implies that the structural quality of the material has not deteriorated after printing. Such printing techniques allow the uniform deposition of plasma-designed graphene structures with desired patterns on any substrates, including metallic, semiconductive or polymeric substrates. Printing process detailed in Supplementary Information.

4. Conclusions

The developed method and the corresponding machine constitute an innovative and disruptive approach to the synthesis of free-standing graphene, N-graphene and related hybrids. This highly versatile machine is distinguished by its ability to perform a wide range of adaptable, industrially relevant synthesis reactions. It achieves gram-scale assembly of free-standing graphene/N-graphene nanosheets and graphene hybrids through a rapid, one-step, continuous and streamlined process at atmospheric pressure, eliminating the need for post-processing or additional chemical treatment. Diverse protocols for selective synthesis of one carbon allotrope, i.e., graphene, have been established, each tailored to distinct carbon and nitrogen precursors. These protocols were used as structured methodologies, to achieve reproducible outcomes in terms of production rate, structural quality (including aspects such as the presence of sp^3 carbons, lateral dimensions, etc.) and chemical composition (such as the presence of oxygen). The key advantage of this method lies in the ability to finely adjust the density and energy of the primary "building units," such as C_2 radicals, C and N atoms, within the high energy-density plasma environment. This precise tuning provides effective control over the energy and material fluxes directed towards the growing nanostructures in the reactor's assembly zone. It is this capability that allows for rigorous control over the synthesis process and predefined outcomes.

Beyond its proficiency in graphene production, the machine serves as a powerhouse for synthesizing diverse hybrid nanomaterials. By leveraging graphene/N-graphene as a conductive matrix for anchoring metal nanoparticles, it establishes a streamlined and efficient method for hybrid nanomaterial synthesis. The machine converts low-cost feedstocks, such as ethanol, methane and acetonitrile, into graphene and derivatives at a production rate of up to 30 mg/min. The resulting N-graphene nanosheets exhibit exceptional quality, featuring the highest reported presence of single atomic layers (approximately 45 %), a high ratio of 2D/G peak intensities in Raman spectra, and an N/O atomic ratio exceeding one. These characteristics attest the well-preserved hexagonal lattice structure of graphene. The plasma's intrinsic thermal and chemical functionalities play a pivotal role, inducing size reduction of micron-sized particles to nanoparticles and conversion into distinct chemical phases. Precision in controlling the size distribution and

chemistry of metal nanoparticles is achieved through the application of various flow regimes of background Ar gas.

What sets this research apart is not only its advancements in nanoscale materials synthesis but also the transformative potential of the presented technology. Beyond the productivity boost, it shows potential to redefine plasma-driven synthesis-by-design, impacting material and energy consumption, cost, and turnaround time. The far-reaching implications span a spectrum of applications, including energy storage and conversion devices, conductive inks, membranes, metamaterials, sensors, and more. The potential value of this novel plasma approach extends beyond the laboratory, presenting unprecedented opportunities for innovation that can drive economic and technological advancements across various industries. Moreover, this technology can be used to synthesize increasingly sophisticated hybrids, seamlessly integrating graphene with semiconductors, magnetic materials, polymers, etc., to unlock synergistic effects, paving the way for the creation of novel materials with significantly enhanced properties. It represents a paradigm shift in the field of 2D materials synthesis, holding the potential to redefine industry benchmarks and stand out as a game-changing innovation in the landscape of graphene production.

CRediT authorship contribution statement

Ana Dias: Data curation, Formal analysis, Investigation, Methodology, Validation, Visualization, Writing – original draft, Writing – review & editing. **Edgar Felizardo:** Investigation, Methodology, Software, Validation, Writing – original draft, Writing – review & editing. **Neli Bundaleska:** Formal analysis, Writing – original draft, Writing – review & editing. **Miroslav Abrashev:** Data curation, Formal analysis, Investigation, Methodology, Writing – original draft. **Jivko Kissovski:** Data curation, Formal analysis, Investigation, Methodology, Writing – original draft. **Ana M. Ferraria:** Data curation, Formal analysis, Funding acquisition, Investigation, Methodology, Writing – original draft. **Ana M. Rego:** Data curation, Formal analysis, Funding acquisition, Investigation, Methodology, Writing – original draft. **Thomas Strunskus:** Data curation, Formal analysis, Investigation, Methodology, Writing – original draft. **Patrícia A. Carvalho:** Data curation, Formal analysis, Investigation, Methodology, Writing – original draft. **Amélia Almeida:** Data curation, Formal analysis, Investigation, Methodology, Writing – original draft. **Janez Zavašnik:** Data curation, Formal analysis, Investigation, Methodology, Writing – original draft. **Eva Kovacevic:** Data curation, Formal analysis, Investigation, Methodology, Writing – original draft. **Johannes Berndt:** Data curation, Formal analysis, Investigation, Methodology, Writing – original draft. **Nenad Bundaleski:** Data curation, Formal analysis, Investigation, Methodology, Writing – original draft. **Mohammed-Ramzi Ammar:** Data curation, Formal analysis, Investigation, Methodology, Writing – original draft. **Orlando M.N.D. Teodoro:** Data curation, Formal analysis, Investigation, Methodology, Writing – original draft. **Uroš Cvelbar:** Data curation, Formal analysis, Methodology, Investigation, Writing – original draft. **Luís L. Alves:** Funding acquisition, Project administration, Resources. **Bruno Gonçalves:** Funding acquisition, Project administration, Resources. **Elena Tatarova:** Conceptualization, Funding acquisition, Methodology, Project administration, Resources, Supervision, Writing – original draft, Writing – review & editing.

Declaration of competing interest

The authors declare that they have no known competing financial interests or personal relationships that could have appeared to influence the work reported in this paper.

Data availability

Data will be made available on request.

Acknowledgements

This work was performed in the framework of the PEGASUS (Plasma Enabled and Graphene Allowed Synthesis of Unique nano-Structures) project, funded by European Union's Horizon 2020 research and innovation program under grant agreement No 766894. Work partially funded by Portuguese FCT - Fundação para a Ciência e a Tecnologia, through project Eager (PTDC/NAN-MAT/30565/2017), iBB and i4HB projects (UIDB/04565/2020, UIDP/04565/2020 and LA/P/0140/2020), and strategic projects UIDB/50010/2020 and UIDP/50010/2020, CEFITEC project LOWSEY (CERN/FIS-TEC/0039/2019), strategic projects (UIDB/00068/2020 and UIDP/00068/2020) and CeFEMA Project UID/CTM/04540/2020. A.M. Ferraria thanks Instituto Superior Técnico for Scientific Employment contract IST-ID/131/2018. F.M. Dias, and I. Dionisio are acknowledged for technical assistance. A. Jagodar, A. Stolz, N. M. Santosh are acknowledged for their assistance regarding graphene printing. The authors would like to thank HZB for the allocation of synchrotron radiation beam time at Bessy II via projects 222-11637-ST and 221-10805-ST on HE-SGM beamline with PREVAC endstation as well as the personnel at BESSY II, for support during our activities at the HE-SGM beamline, and Professor Dr. Ch. Wöll and Dr. A. Nefedov for providing the endstation.

Supplementary materials

Supplementary material associated with this article can be found, in the online version, at doi:10.1016/j.apmt.2024.102056.

References

[1] M.A. Al Faruque, M. Syduzzaman, J. Sarkar, K. Bilisik, M. Naebe, A Review on the Production Methods and Applications of Graphene-Based Materials, Nanomaterials 11 (2021) 2414, https://doi.org/10.3390/nano11092414.
[2] N.T. Padmanabhan, N. Thomas, J. Louis, D.T. Mathew, P. Ganguly, H. John, S. C. Pillai, Graphene coupled TiO_2 photocatalysts for environmental applications: A review, Chemosphere 271 (2021) 129506, https://doi.org/10.1016/j.chemosphere.2020.129506.
[3] L. Lin, H. Peng, Z. Liu, Synthesis challenges for graphene industry, Nat. Mater. 18 (2019) 520, https://doi.org/10.1038/s41563-019-0341-4.
[4] A.P. Kauling, A.T. Seefeldt, D.P. Pisoni, R.C. Pradeep, R. Bentini, R.V.B. Oliveira, K. S. Novoselov, A.H. Castro Neto, The Worldwide Graphene Flake Production, Adv. Mater. 30 (2018) 1803784, https://doi.org/10.1002/adma.201803784.
[5] M. Yi, Z. Shen, A review on mechanical exfoliation for the scalable production of graphene, J. Mater. Chem. A 3 (2015) 11700–11715, https://doi.org/10.1039/C5TA00252D.
[6] Y. Hernandez, V. Nicolosi, M. Lotya, F.M. Blighe, Z. Sun, S. De, I.T. McGovern, B. Holland, M. Byrne, Y.K. Gun'Ko, J.J. Boland, P. Niraj, G. Duesberg, S. Krishnamurthy, R. Goodhue, J. Hutchison, V. Scardaci, A.C. Ferrari, J. N. Coleman, High-yield production of graphene by liquid-phase exfoliation of graphite, Nat. Nanotechnol. 3 (2008) 563–568, https://doi.org/10.1038/nnano.2008.215, 2008.
[7] X. Li, C.W. Magnuson, A. Venugopal, R.M. Tromp, J.B. Hannon, E.M. Vogel, L. Colombo, Rodney S. Ruoff, Large-Area Graphene Single Crystals Grown by Low-Pressure Chemical Vapor Deposition of Methane on Copper, J. Am. Chem. Soc. 133 (2011) 2816–2819, https://doi.org/10.1021/ja109793s.
[8] X. Wang, G. Sun, P. Routh, D.-H. Kim, W. Huang, Heteroatom-doped graphene materials: syntheses, properties and applications, Chem. Soc. Rev. 43 (2014) 7067, https://doi.org/10.1039/C4CS00141A.
[9] H. Wang, T. Maiyalagan, Xin Wang, Review on recent progress in nitrogen-doped graphene: synthesis, characterization, and its potential applications, ACS Catal 2 (2012) 781–794, https://doi.org/10.1021/cs200652y.
[10] Y. Ito, C. Christodoulou, M.V. Nardi, N. Koch, H. Sachdev, K. Müllen, Chemical vapour deposition of N-doped graphene and carbon films. The role of precursors and gas phase, ACS Nano 8 (2014) 3337–3346, https://doi.org/10.1021/nn405661b.
[11] D. Deng, X. Pan, L. Yu, Y. Cui, Y. Jiang, J. Qi, W.-X Li, Q. Fu, X. Ma, Q. Xue, G. Sun, X. Bao, Toward N-doped graphene via solvothermal synthesis, Chem. Mater. 23 (2011) 1188–1193, https://doi.org/10.1021/cm102666r.
[12] Z. Lin, G. Waller, Y. Liu, M. Liu, C.-P. Wong, Facile synthesis of nitrogen doped graphene via pyrolysis of graphene oxide and urea, and its electrocatalytic activity toward the oxygen reduction reaction, Adv. Energy Mater. 2 (2012) 884–888, https://doi.org/10.1002/aenm.201200038.
[13] W.S. Hummers, R.E. Offeman, Preparation of graphitic oxide, J. Am Chem. Soc. 80 (1958) 1339, https://doi.org/10.1021/ja01539a017.
[14] A. Islam, B. Mukherjee, K.K. Pandey, A.K. Keshri, Ultra-Fast, Chemical-Free, Mass Production of High Quality Exfoliated Graphene, ACS Nano 15 (2021) 1775, https://doi.org/10.1021/acsnano.0c09451.

[15] V.V. Slezov, A.S. Abyzov, Z.V. Slezova, Kinetics of the phase separation of a low-viscosity liquid supersaturated with gas at the intermediate and later stages, Colloid J 67 (2005) 85–96, https://doi.org/10.1007/PL00021814.

[16] M. Bahri, S.H. Gebre, M.A. Elaguech, F.T. Dajan, M.G. Sendeku, C. Tlili, D. Wang, Recent advances in chemical vapour deposition techniques for graphene-based nanoarchitectures: From synthesis to contemporary applications, Coordination Chemistry Reviews 475 (2023) 214910, https://doi.org/10.1016/j.ccr.2022.214910.

[17] J.M. Lehn, Perspectives in Chemistry - Aspects of Adaptive Chemistry and Materials, Angew. Chemie - Int, Ed. 54 (2015) 3276–3289, https://doi.org/10.1002/anie.201409399.

[18] D. Tsyganov, N. Bundaleska, A. Dias, J. Henriques, E. Felizardo, M. Abrashev, J. Kissovski, A.M.B. Do Rego, A.M. Ferraria, E. Tatarova, Microwave plasma-based direct synthesis of free-standing N-graphene, Phys. Chem. Chem. Phys. 22 (2020) 4772–4787, https://doi.org/10.1039/C9CP05509F.

[19] E. Tatarova, A. Dias, J. Henriques, M. Abrashev, N. Bundaleska, E. Kovacevic, N. Bundaleski, U. Cvelbar, E. Valcheva, B. Arnaudov, A.M.B. Do Rego, A. M. Ferraria, J. Berndt, E. Felizardo, O.M.N.D. Teodoro, T. Strunskus, L.L. Alves, B. Gonçalves, Towards large-scale in free-standing graphene and N-graphene sheets, Sci. Rep. 7 (2017) 10175, https://doi.org/10.1038/s41598-017-10810-3.

[20] N. Bundaleska, D. Tsyganov, A. Dias, E. Felizandro, J. Henriques, F.M. Dias, M. Abrashev, J. Kissovski, E. Tatarova, Microwave plasma enabled synthesis of free standing carbon nanostructures at atmospheric pressure conditions, Phys. Chem. Chem. Phys. 20 (2018) 13810–13824, https://doi.org/10.1039/C8CP01896K.

[21] X. Wang, G. Sun, P. Routh, D.-H. Kim, W. Huang, Peng Chen, Heteroatom-doped graphene materials: syntheses, properties and applications, Chem. Soc. Rev. 43 (2014) 7067, https://doi.org/10.1039/C4CS00141A.

[22] H. Wang, T. Maiyalagan, X. Wang, Review on Recent Progress in Nitrogen-Doped Graphene: Synthesis, Characterization, and Its Potential Applications, ACS Catal 2 (5) (2012) 781–794, https://doi.org/10.1021/cs200652y.

[23] P. Arias-Monje S. K. Menon, H. Zea, S. Osswald, C.C. Luhrs, Nitrogen doped graphene generated by microwave plasma and reduction expansion synthesis, Nanosci. Nanotech. Let. 8 (2016) 120–128, https://doi.org/10.1166/nnl.2016.2055.

[24] D.X. Luong, K.V. Bets, W.A. Algozeeb, M.G. Stanford, C. Kittrell, W. Chen, R. V. Salvatierra, M. Ren, E.A. McHugh, P.A. Advincula, Z. Wang, M. Bhatt, H. Guo, V. Mancevski, R. Shahsavari, B.I. Yakobson, J.M. Tour, Gram-scale bottom-up flash graphene synthesis, Nature 577 (7792) (2020) 647–651, https://doi.org/10.1038/s41586-020-1938-0.

[25] D. Kurniawan, W.-H. Chiang, Microplasma-enabled colloidal nitrogen-doped graphene quantum dots for broad-range fluorescent pH sensors, Carbon 167 (2020) 675e684, https://doi.org/10.1016/j.carbon.2020.05.085.

[26] W.-H. Chiang, D. Mariotti, R.M. Sankaran, J.G. Eden, K. Ostrikov, Microplasmas for Advanced Materials and Devices, Adv. Mater. 32 (2020) 1905508, https://doi.org/10.1002/adma.201905508.

[27] X.-F. Luo, S.-Y. Wang, C.-M. Tseng, S.-W. Lee, W.-H. Chiang, J.-K. Chang, Microplasma-assisted bottom-up synthesis of graphene nanosheets with superior sodium-ion storage performance, J. Mater. Chem. A 4 (2016) 7624–7631, https://doi.org/10.1039/C6TA00743K.

[28] Z.-S. Wu, G. Zhou, L.-C. Yin, W. Ren, F. Li, H.-M. Cheng, Graphene/metal oxide composite electrode materials for energy storage, Nano Energy 1 (2012) 107–131, https://doi.org/10.1016/j.nanoen.2011.11.001.

[29] M. Beidaghi, C. Wang, Micro-Supercapacitors Based on Interdigital Electrodes of Reduced Graphene Oxide and Carbon Nanotube Composites with Ultrahigh Power Handling Performance, Advanced Functional Materials 22 (2012) 4501–4510, https://doi.org/10.1002/adfm.201201292.

[30] Y. Wang, Y. Wu, Y. Huang, F. Zhang, X. Yang, Y. Ma, Y. Chen, Preventing Graphene Sheets from Restacking for High-Capacitance Performance, J. Phys. Chem. C 115 (46) (2011) 23192–23197, https://doi.org/10.1021/jp206444e.

[31] Q. Cheng, J. Tang, J. Ma, H. Zhang, N. Shinya, L.-C. Qin, Graphene and carbon nanotube composite electrodes for supercapacitors with ultra-high energy density, Phys. Chem. Chem. Phys. 13 (2011) 17615–17624, https://doi.org/10.1039/C1CP21910C.

[32] M. Khan, M.N. Tahir, S.F. Adil, H.U. Khan, M.R.H. Siddiqui, A.A. Al-warthan, W. Tremel, Graphene based metal and metal oxide nanocomposites: synthesis, properties and their applications, J Mater Chem A 3 (2015) 18753, https://doi.org/10.1039/C5TA02240A.

[33] Q. Lai, Y. Zhao, J. Zhu, Y. Liang, J. He, Directly Anchoring Highly Dispersed Copper Sites on Nitrogen-Doped Carbon for Enhanced Oxygen Reduction Electrocatalysis, J. Chen. Chem Electro Chem 5 (2018) 1822, https://doi.org/10.1002/celc.201800058.

[34] G. Yuan, J. Xiang, H. Jin, L. Wu, Y. Jin, Y. Zhao, Anchoring ZnO Nanoparticles in Nitrogen-Doped Graphene Sheets as a High-Performance Anode Material for Lithium-Ion Batteries, Materials 11 (2018) 1, https://doi.org/10.3390/ma11010096.

[35] H. Wang, C. Jiang, C. Yuan, Q. Wu, Q. Li, Q. Duan, Complexing agent engineered strategy for anchoring SnO2 nanoparticles on sulfur/nitrogen co-doped graphene for superior lithium and sodium ion storage, Chemical Engineering Journal 332 (2018) 237–244, https://doi.org/10.1016/j.cej.2017.09.081.

[36] C. Hu, T. Lu, F. Chen, A brief review of graphene–metal oxide composites synthesis and applications in photocatalysis, J. Chinese Adv. Mater. Soc. 1 (1) (2013) 21, https://doi.org/10.1080/22243682.2013.771917.

[37] Z. Ma, H. Cao, X. Zhou, W. Deng, Z. Liu, Hierarchical porous MnO/graphene composite aerogel as high-performance anode material for lithium ion batteries, RSC Adv 7 (2017) 15857, https://doi.org/10.1039/C7RA00818J.

[38] J. Duan, S. Chen, S. Dai, S.Z. Qiao, Shape Control of Mn3O4 Nanoparticles on Nitrogen-Doped Graphene for Enhanced Oxygen Reduction Activity, Adv. Funct. Mater. 24 (2014) 2072–2078, https://doi.org/10.1002/adfm.201302940.

[39] K. Zhang, P. Han, L. Gu, L. Zhang, Z. Liu, Q. Kong, C. Zhang, S. Dong, Z. Zhang, Jianhua Yao†, H. Xu, G. Cui, L. Chen, Synthesis of Nitrogen-Doped MnO/Graphene Nanosheets Hybrid Material for Lithium Ion Batteries, ACS Appl. Mater. Interfaces 4 (2) (2012) 658, https://doi.org/10.1021/am201173z.

[40] R. Chen, J. Yan, Y. Liu, J. Li, Three-Dimensional Nitrogen-Doped Graphene/MnO Nanoparticle Hybrids as a High-Performance Catalyst for Oxygen Reduction Reaction, J. Phys. Chem. C 119 (2015) 8032–8037, https://doi.org/10.1021/acs.jpcc.5b00306.

[41] A. Jana, E. Scheer, S. Polarz, Synthesis of graphene–transition metal oxide hybrid nanoparticles and their application in various fields J, Nanotechnol. 8 (2017) 688–714, https://doi.org/10.3762/bjnano.8.74.

[42] Z. Li, J. Wang, S. Liu, X. Liu, S. Yang, J. Power Sources 196 (2011) 8160–8165, https://doi.org/10.1016/j.jpowsour.2011.05.036.

[43] X.Y. Zhang, H.P. Li, X.L. Cui, Y.H. Lin, Synthesis of hydrothermally reduced graphene/MnO2 composites and their electrochemical properties as supercapacitors, J Mater Chem 20 (2010) 2801, https://doi.org/10.1016/j.jpowsour.2011.05.036.

[44] J. Du, X.Y. Lai, N. Yang, J. Zhai, D. Kisailus, F. Su, D. Wang, L. Jiang, Hierarchically ordered macro-mesoporous TiO_2-graphene composite films: improved mass transfer, reduced charge recombination, and their enhanced photocatalytic activities, ACS Nano 5 (2011) 590, https://doi.org/10.1021/nn102767d.

[45] D. Wang, D. Choi, J. Li, Z. Yang, Z. Nie, R. Kou, D. Hu, C. Wang, L.V. Saraf, J. Zhang, I.A. Aksay, J. Liu, Self-assembled TiO2-graphene hybrid nanostructures for enhanced Li-ion insertion, ACS Nano 3 (2009) 907, https://doi.org/10.1021/nn900150y.

[46] G. Zhou, D.-W. Wang, F. Li, L. Zhang, N. Li, Z.-S. Wu, L. Wen, G.Q. Lu, H.-M. Cheng, Graphene-Wrapped Fe3O4 Anode Material with Improved Reversible, Capacity and Cyclic Stability for Lithium Ion Batteries, Chem. Mater. 22 (2010) 5306–5313, https://doi.org/10.1021/cm101532x.

[47] S. Yang, X. Feng, L. Wang, K. Tang, J. Maier, K. Müllen, Graphene-based nanosheets with a sandwich structure, Angew. Chem. Int. Ed. 49 (2010) 4795, https://doi.org/10.1002/anie.201001634.

[48] J.F. Shen, C. Yan, M. Shi, H.W. Ma, N. Li, M.X. Ye, One step hydrothermal synthesis of TiO2-reduced graphene oxide sheets, J. Mater. Chem. 21 (2011) 3415, https://doi.org/10.1039/C0JM03542D.

[49] B.J. Jiang, C.G. Tian, Q.J. Pan, Z. Jiang, J.Q. Wang, W.S. Yan, H.G. Fu, Enhanced photocatalytic activity and electron transfer mechanisms of graphene/TiO2 with exposed {001} facets, J. Phys. Chem. C. 115 (2011) 23718, https://doi.org/10.1021/jp207624x.

[50] J.Z. Wang, C. Zhong, D. Wexler, N.H. Idris, Z.X. Wang, L.Q. Chen, H.K. Liu, Graphene-encapsulated Fe3O4 nanoparticles with 3D laminated structure as superior anode in lithium ion batteries, Chem. Eur. J. 17 (2011) 661, https://doi.org/10.1002/chem.201001348.

[51] J.X. Zhu, Y.K Sharma, Z.Y. Zeng, X.J. Zhang, M. Srinivasan, S. Mhaisalkar, H. Zhang, H.H. Hng, Q.Y. Yan, Cobalt Oxide Nanowall Arrays on Reduced Graphene Oxide Sheets with Controlled Phase, Grain Size, and Porosity for Li-Ion Battery Electrodes, J. Phys. Chem. C 115 (2011) 8400, https://doi.org/10.1021/jp2002113.

[52] H. Raj, A. Sil, N.V. Pulagara, MnO anchored reduced graphene oxide nanocomposite for high energy applications of Li-ion batteries: The insight of charge-discharge process, Ceramics International 45 (2019) 14829–14841, https://doi.org/10.1016/j.ceramint.2019.04.214.

[53] D.H. Wang, R. Kou, D.W. Choi, Z. Yang, Z. Nie, J. Li, L.V. Saraf, D. Hu, J. Zhang, Gordon L. Graff, J. Liu, M.A. Pope, I.A. Aksay, Ternary self-assembly of ordered metal oxide-graphene nanocomposites for electrochemical energy storage, ACS Nano 4 (2010) 1587, https://doi.org/10.1021/nn901819n.

[54] J. Yan, Z.J. Fan, T. Wei, W.Z. Qian, M. Zhang, F. Wei, Fast and reversible surface redox reaction of graphene-MnO2 composites as supercapacitor electrodes, Carbon 48 (2010) 3825, https://doi.org/10.1016/j.carbon.2010.06.047.

[55] J. Yan, T. Wei, W.M. Qiao, B. Shao, Q.K. Zhao, L.J. Zhang, Z.J. Fan, Rapid microwave-assisted synthesis of graphene nanosheet/Co3O4 composite for supercapacitors, Electrochimica Acta 55 (2010) 6973, https://doi.org/10.1016/j.electacta.2010.06.081.

[56] S.X. Wu, Z.Y. Yin, Q.Y. He, X. Huang, X.Z. Zhou, H. Zhang, Electrochemical deposition of semiconductor oxides on reduced graphene oxide-based flexible, transparent, and conductive electrodes, J. Phys. Chem. C 114 (2010) 11816, https://doi.org/10.1021/jp103696u.

[57] Z.Y. Yin, S.X. Wu, X.Z. Zhou, X. Huang, Q.C. Zhang, F. Boey, H. Zhang, Electrochemical deposition of ZnO nanorods on transparent reduced graphene oxide electrodes for hybrid solar cells, Small 6 (2010) 307, https://doi.org/10.1002/smll.200901968.

[58] F. Ji, Y.-L. Li, J.-M. Feng, D. Su, Y.-Y. Wen, Y. Feng, F. Hou, Electrochemical performance of graphene nanosheets and ceramic composites as anodes for lithium batteries, J. Mater. Chem. 9 (2009) 9063, https://doi.org/10.1039/B915838C.

[59] J.T. Zhang, Z.G. Xiong, X.S. Zhao, Graphene–metal–oxide composites for the degradation of dyes under visible light irradiation, J. Mater. Chem. 21 (2011) 3634, https://doi.org/10.1039/C0JM03827J.

[60] E. Tatarova, J. Henriques, L. Alves, B. Gonçalves, (IST), Processo para a produção de materiais nanocompósitos em reator único utilizando tecnologia plasma, PT 115782 B (2021). https://patentscope.wipo.int/search/en/detail.jsf?docId=PT321230609&_cid=P12-L2RJJN-73238-1.

[61] E. Tatarova, J. Henriques, L. Alves, B. Gonçalves, (IST), Process, reactor and system for fabrication of freestanding two-dimensional nanostructures using plasma

technology, PT 110764 (2021). https://patentscope.wipo.int/search/en/detail.jsf?docId=WO2017196198.
[62] E. Tatarova, J. Henriques, L. Alves, B. Gonçalves, (IST), Process, reactor and system for fabrication of freestanding two-dimensional nanostructures using plasma technology, US 11254575B2 (2022). https://patentscope.wipo.int/search/en/detail.jsf?docId=US293705927&_fid=WO2017196198.
[63] E. Tatarova, J. Henriques, L. Alves, B. Gonçalves, (IST), Processo, reator e sistema para a produção seletiva de nanoestruturas bidimensionais autónomas utilizando tecnologia plasma, PT 109387 (2021). https://patentscope.wipo.int/search/en/detail.jsf?docId=PT232851188&_fid=WO2017196198.
[64] E. Tatarova, J. Henriques, L. Alves, B. Gonçalves, (IST), Reactor for fabrication of graphene, EP 3567130 (2022) published, https://patentscope.wipo.int/search/en/detail.jsf?docId=EP276408838&_fid=PT232851188.
[65] M. Moisan, M. Chaker, Z. Zakrzewski1, J Paraszczak, J. Phys. E: Sci. Instrum. 20 (1987) 1356, https://doi.org/10.1088/0022-3735/20/11/009.
[66] Z.Q. Li, C.J. Lu, Z.P. Xia, Y. Zhou, Z. Luo, X-ray diffraction patterns of graphite and turbostratic carbon, Carbon 45 (2007) 1686–1695, https://doi.org/10.1016/j.carbon.2007.03.038.
[67] N. Bundaleska, A. Dias, N. Bundaleski, E. Felizardo, J. Henriques, D. Tsyganov, M. Abrashev, E. Valcheva, J. Kissovski, A.M. Ferraria, A.M. Botelho do Rego, A. Almeida, J. Zavašnik, U. Cvelbar, O.M.N.D. Teodoro, Th. Strunskus, E. Tatarova, Prospects for microwave plasma synthesized N-graphene in secondary electron emission mitigation applications, Scientific Reports 10 (2020) 13013, https://doi.org/10.1038/s41598-020-69844-9.
[68] S.A. Evlashin, F.S. Fedorov, P.V. Dyakonov, Y.M. Maksimov, A.A. Pilevsky, K. I. Maslakov, Y.O. Kuzminova, Y.A. Mankelevich, E.N. Voronina, S.A. Dagesyan, V. A. Pletneva, A.A. Pavlov, M.A. Tarkhov, I.V. Trofimov, V.L. Zhdanov, N.V. Suetin, I.S. Akhatov, Role of nitrogen and oxygen in capacitance formation of carbon nanowalls, J. Phys. Chem. Lett. 11 (2020) 4859–4865, https://doi.org/10.1021/acs.jpclett.0c01274.
[69] S.A. Evlashin, Y.M. Maksimov, P.V. Dyakonov, A.A. Pilevsky, K.I. Maslakov, Y. A Mankelevich, E.N. Voronina, S.V. Vavilov, A.A. Pavlov, E.V. Zenova, I. S. Akhatov, N.V. Suetin, N-doped carbon nanowalls for power sources, Sci. Rep. 9 (2019) 6716, https://doi.org/10.1038/s41598-019-43001-3.
[70] J.P. McClure, J.D Thornton, R.Z Jiang, D. Chu, J.J. Cuomo, P.S. Fedkiw, Oxygen reduction on metal-free nitrogen-doped carbon nanowall electrodes, J. Electrochem. Soc. 159 (2012) F733–F742, https://doi.org/10.1149/2.056211jes.
[71] H.M. Jeong, J.W. Lee, W.H. Shin, Y.J. Choi, H.J. Shin, J.K. Kang, J.W. Choi, Nitrogen-doped graphene for high-performance ultracapacitors and the importance of nitrogen-doped sites at basal planes, Nano Lett 11 (2011) 2472–2477, https://doi.org/10.1021/nl2009058.
[72] G. Singh, D.S. Sutar, V.D. Botcha, P.K. Narayanam, S.S. Talwar, R.S. Srinivasa, S. S. Major, Study of simultaneous reduction and nitrogen doping of graphene oxide Langmuir-Blodgett monolayer sheets by ammonia plasma treatment, Nanotechnol 24 (2013) 11, https://doi.org/10.1088/0957-4484/24/35/355704.
[73] P.A. Manojkumar, N.G. Krishna, G. Mangamma, S.K. Albert, Understanding the structural and chemical changes in vertical graphene nanowalls upon plasma nitrogen ion implantation, Phys. Chem. Chem. Phys. 21 (2019) 10773–10783, https://doi.org/10.1039/C9CP02165E.
[74] M. Coros, C. Varodi, F. Pogacean, E. Gal, S.M. Pruneanu, Nitrogen-Doped Graphene: The Influence of Doping Level on the Charge-Transfer Resistance and Apparent Heterogeneous Electron Transfer Rate, Sensors 20 (7) (2020) 1815, https://doi.org/10.3390/s20071815.
[75] A. Dias, N. Bundaleski, E. Tatarova, F.M. Dias, M. Abrashev, U. Cvelbar, O.M.N. D. Teodoro, J. Henriques, Production of N-graphene by microwave N2-Ar plasma, J. Phys. D Appl. Phys. 49 (2016) 055307, https://doi.org/10.1088/0022-3727/49/5/055307.
[76] N. Bundaleska, J. Henriques, M. Abrashev, A.M. Botelho do Rego, A.M. Ferraria, A. Almeida, F.M. Dias, E. Valcheva, B. Arnaudov, K.K. Upadhyay, M.F. Montemor, E. Tatarova, Large-scale synthesis of free-standing N-doped graphene using microwave plasma, Sci. Rep. 8 (2018) 12595, https://doi.org/10.1038/s41598-018-30870-3.